Plasma Chem Plasma Process (2010) 30:641–661
DOI 10.1007/s11090-010-9238-3

ORIGINAL PAPER

An Analysis of Low Frequency Discharge in a CH_3SiCl_3-Ar-H_2 Mixture by Optical Emission Spectroscopy and Actinometry

Barbara Kułakowska-Pawlak · Piotr Jamróz

Received: 21 January 2010 / Accepted: 1 June 2010 / Published online: 15 June 2010
© Springer Science+Business Media, LLC 2010

Abstract Low frequency (100 kHz) discharge in Ar-H_2 and CH_3SiCl_3-Ar-H_2 mixtures was studied to obtain information on the processes involved in plasma deposition of Si_xC_y:H films from CH_3SiCl_3-Ar-H_2 plasma once the properties of Ar-H_2 plasma are known. The plasmas were studied using optical emission spectroscopy. The addition of small amounts of nitrogen to the plasma mixtures also permitted the use of an actinometry technique. First, plasma parameters (electron density and temperature) and actinometric concentrations of atomic hydrogen in an argon–hydrogen plasma were investigated as a function of the hydrogen content in the feed. Second, the emission intensities of Si, Si^+, CH, H, Ar and Ar^+ species produced in the CH_3SiCl_3-Ar-H_2 discharge were analysed as a function of time following the introduction of CH_3SiCl_3 (methyltrichlorosilane, MTCS) to the argon–hydrogen plasmas with various proportions of the feed gasses. The results reveal a rapid decay of the Si-excited state number density versus time, while those of Si^+ and CH fell off more slowly. The emission of atomic silicon was believed to be a result of electron impact dissociative and excitation processes occurring in the bulk of the discharge, whereas the Si^+ and CH seemed to originate mainly from products of sputtering of the growing film surface. The fragmentation of the MTCS associated with HCl formation and enhanced atomic hydrogen production as a result of HCl dissociation are proposed. Variations in the radical densities of H and CH_3 were determined using an actinometry technique. The results indicate a significant role for H_2 in gas-phase reactions occurring in the CH_3SiCl_3-Ar-H_2 plasma, as well as in gas-surface interactions, leading to competition between deposition and chemical sputtering of already deposited material.

Keywords Methyltrichlorosilane · Emission spectroscopy · Gas phase reaction · Plasma CVD

B. Kułakowska-Pawlak (✉) · P. Jamróz
Faculty of Chemistry, Wrocław University of Technology, 50-370 Wrocław, Poland
e-mail: barbara.kulakowska-pawlak@pwr.wroc.pl

Introduction

Films based on hydrogenated silicon carbide, Si_xC_y:H, are characterised by exceptional optical, electrical and thermal properties [1], giving them a wide range of practical application. The films are usually prepared by chemical vapour deposition or by plasma assisted chemical vapour deposition (PACVD) techniques operating with silane and methane gas mixures [2, 3]. A promising alternative to silane, as an explosive gas, is the use of volatile chlorine-containing organosilicon compounds containing both silicon and carbon. Methyltrichlorosilane (CH_3SiCl_3, MTCS) belongs to this class of precursor. MTCS is the most chemically reactive compound among the chloroalkylosilanes. It is relatively cheap and inexplosive. The further advantage of using MTCS is its high room-temperature vapour pressure (17.9 kPa), which makes it easy to use in vapour deposition processes. Its disadvantage as a precursor in the deposition processes is its large chlorine content, the build-up of which in films can deteriorate their quality. In such a case, addition of hydrogen to the plasma is beneficial because of its scavenger role on halogen atoms.

An important contribution to the developing technology of preparing Si_xC_y:H coatings by PACVD from MTCS diluted in hydrogen was made by a group of Ukrainian researchers [4–8]. They used a non-standard plasmochemical installation with a high frequency (40.7 MHz) plasma generator. Their studies concentrated on the major technological parameters and their effects on microstructure [4–6] and chemical composition [5] and hence on the electronic [4, 5], tribological [7, 8] and mechanical [6] properties of the deposit. Among other things, it was established that the ratio of the MTCS and H_2 concentrations strongly affected the film structures [4]. They found that the carbon content in the deposit decreased as the MTCS flow rate and the negative potential on the substrate increased [5, 6]. The carbon content was also reduced with increasing discharge power [5]. They suggested that the growing surface is saturated by silicon-based species as a result of etching out weakly bonded CH_x radicals [5].

Various techniques for film analysis and optical emission spectroscopy (OES) for plasma investigation were applied by Kaneko et al. [9, 10] to study the growth mechanism of a-SiC:H films produced in a PACVD process using MTCS and H_2 (RF of 13.56 MHz). They observed OES signals from H and H_2 and very weak signals from $SiCl_2$ emission that increased in intensity with the power plasma density (or electron density). The atomic ratio of Si:C in the films was found to be higher at higher power densities. The conclusion of Kaneko et al. [9] was that competition between decomposition of $SiCl_3$ and CH_3 was responsible for the film composition.

To the best of the authors' knowledge, with the exception of the cited results of the OES studies of Kaneko et al., no attempt has been made so far to obtain information on the gas phase species in this deposit system. It is evident that more complete knowledge of the discharge chemistry is necessary in order to develop existing applications and optimise the properties and structure of the deposits generated from the decomposition of MTCS in the plasma. The present study is related to this research problem. In the following research, OES was used to investigate the natures and densities of species formed by a low-frequency discharge in a mixture of CH_3SiCl_3, H_2, Ar and N_2. Methyltrichlorosilane and hydrogen were the reactive compounds. Argon acted as a dilution gas, and N_2 was present only in a small proportion to allow for quantitative optical emission spectroscopy (actinometry) of the discharge. The total pressure was constant. The H_2 amount in the gas feed was chosen as the experimental variable. Depending on the concentration of hydrogen added in the gas feed, modifications of the plasma reactivity and the plasma surface interaction were to be expected.

OES is an in situ nonintrusive technique for the detection of electronically excited atoms, ions and di- or triatomic molecules. These excited species decay and emit light at characteristic wavelengths. The intensities of the emitting spectral per se do not normally allow for conclusions to be drawn about the number densities of particles in their ground states unless the excitation and competing quenching mechanisms are known. However, if a number of assumptions are fulfilled [11–14], emission features can be applied to determine relative changes in the ground state concentration [X] of various species of interest, X, in the plasma source by using a simple actinometric equation [11]:

$$[X] = k(I_X/I_A) \quad (1)$$

where k is a constant and I_X and I_A are the emission intensities of the species, X, and of the actinometer (probe gas), which has a constant concentration in the plasma. Strictly speaking, the actinometric procedure may be only applied under the following conditions: the electronic excitation from the electron impacts and the decay of the excited species by photoemission can be established; the threshold energies, E_{th}, for excitation to the state responsible for the emission is the same in both X and A; and the excitation efficiencies of the two species have a similar dependence on the plasma parameters. In practice, all of these requirements are rarely met because of the lack of choice of actinometers. Argon is usually used as an actinometer ($\lambda = 750$ nm, $E_{th} = 13,5$ eV), but argon was the major carrier gas in our study. Consequently, in the present study, N_2 was employed as an actinometer. The threshold energy for the $N_2(C^3\Pi)$ excited state is 11.2 eV, which is reasonably close to that of the species of interest in discharges such as H ($E_{th} \sim 12$ eV) and CH ($\sim$11 eV).

This work is composed of two main parts. In the first part, we focus on simpler glow discharge plasmas of the Ar-H_2 mixture before addressing, in the second part, the more complex issues associated with the introduction of methyltrichlorosilane to the argon–hydrogen plasma.

The optical emission spectrum of an Ar-H_2 plasma was used to examine some of the elemental processes affecting the populations of excited species in the plasma and for estimating the variations of the plasma parameters (electron density, electron temperature) as functions of the operating conditions (argon/hydrogen ratio, discharge current). In particular, the validity of the basic assumptions of N_2 actinometry for H-atoms is analysed.

In the second part of the work we examine the concentrations of the excited species, the concentrations of atomic hydrogen and the CH_3 radical (as determined by actinometry), and electron density as a function of H_2 content in an MTCS-Ar-H_2 plasma and experimental time ratio.

Experimental

The experimental setup used was that described in detail elsewhere [15]. Two flat steel electrodes with different diameters (20 and 16 mm) were connected to a mid-frequency (100 kHz) power supply operating in constant-current mode (maximum power density about 50 W/cm^2). The distance between the electrodes was about 15 mm. The smaller, powered electrode was covered with a plate that tightly enclosed the walls of the electrode. The plate was made of Armco-steel and was replaced after each of the experiments with a CH_3SiCl_3-Ar-H_2 mixture. After each series of runs, all inner reactor surfaces were cleaned. Methyltrichlorosilane (Aldrich made, 99.9% purity) vapour was admitted into the Ar-H_2

mixture from a glass container sealed by a Teflon needle valve. Argon and hydrogen flows were adjusted by needle valves and flowmeters (ERG 50). Nitrogen was fed through a calibrated flowmeter (Tylan General). The total pressure was measured with a Compact FullRange gauge (Pfeiffer PKR 251). The set up was equipped with a liquid-nitrogen trap, which prevented the reflux of unused gases from entering the reaction chamber.

During the experiments with an argon–hydrogen plasma (without of MTCS), the total pressure in the chamber was set to 665 Pa (5 Torr). The pressure of N_2 (actinometer gas) was about 3% of the total pressure. The partial pressure of hydrogen in the mixture (p_{H2}/ (p_{H2} + $p_{Ar)}$), hereafter x(H_2), and the discharge current were independently changed. The x(H_2) was varied over the range of 0.09–0.45. The current was 70, 100 or 120 mA.

The experiments with the CH_3SiCl_3-Ar-H_2 (+N_2) mixture were carried out with the total pressure of an argon–hydrogen(+nitrogen) mixture controlled at 665 Pa (± 1%) and with the x(H_2) set at 0.1, 0.2 or 0.4. When the gas and pressure conditions were at the desired set points, the discharge was ignited, and the MTCS was then delivered into the reaction chamber. The pressure in the chamber initially increased uncontrollably because the precursor feed rate at the initial stage was high (as a result of the pressure difference between the chamber and the container at the beginning of the experiment). The pressure decreased to a constant level after a few minutes. Throughout this study, the mean MTCS flow was about 0.015 g min^{-1} (estimated gravimetrically) which resulted in a stable total pressure in the reactor of 732 Pa (5.5 Torr) after about 5 min following the introduction of MTCS to the reactor.

In the case of experiments with MTCS, we restricted our measurements to one level of discharge current, namely 100 mA. The reason for this was the low level of optical emission at 70 mA and the instability of the discharge under a discharge current of 120 mA.

Emission spectroscopy measurements were performed perpendicularly to the discharge axis through a quartz window at the end of a lateral tube. A positive lens imaged the most luminous discharge region, close to the powered electrode, onto the monochromator slit (50 μm). A Bentham M-300 h scanning monochromator equipped with a 1800-groove/mm grating (dyspersion of 1.8 nm/mm, spectral resolution 0.15 nm) and a Hamamatsu DH-3 photomultiplier was used. To estimate the electron number density (from Stark broadening of H_β line), the experimental profile of the H_β line was measured in the second order using a high resolution PGS-2 spectrograph.

The spectra of an argon–hydrogen plasma were recorded in the spectral range from 450 to 820 nm. In the case of experiments with MTCS, the spectra were taken at a few short wavelength intervals to minimise the measurement times. Differences in the sensitivity of the recording system over a wide range of wavelengths were corrected by measuring the intensity of a tungsten ribbon lamp (Bentham CL2) with a Protection Engineering certificate.

Results and Discussion

Ar-H_2 Plasma System

The emission spectrum of the glow discharge in the argon/hydrogen mixture consisted of atomic and ionic lines of argon, lines of hydrogen and a few lines belonging to the spectrum of molecular hydrogen. Figure 1 shows typical spectrum of the Ar-H_2 plasma in the 650–760-nm wavelength region. After nitrogen (actinometer) was introduced, bands of

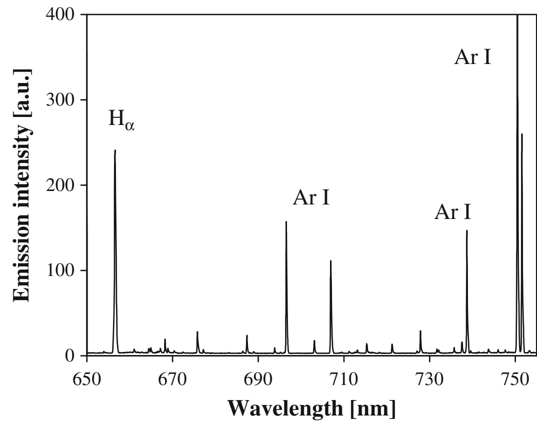

Fig. 1 Typical emission spectra from the Ar-H_2 plasma in the 650–760-nm wavelength region

N_2, N_2^+ and NH molecules appeared. Some of the Ar I, Ar II, and H lines and N_2 bands were selected for diagnostics of the plasma. Their characteristics are given in Table 1.

Three independent runs of the OES measurements for hydrogen amounts, x(H_2), ranging from 0.09 to 0.45 were performed. The discharge was then operated at a constant total pressure of 665 Pa and 100 mA. The error in reproducibility of the emission measurements was less than 5%. Figure 2 presents the dependencies of emission intensities of atomic hydrogen, Ar I, Ar II and N_2 versus x(H_2). One can see that, as expected, the emission intensities of the H_α line increased with the amount of H_2 feed. The increase was a factor of 2.5, for an increase in x(H_2) of a factor of 5.

As the percentage of argon decreased with increasing x(H_2), the intensity of the 750.4–nm line of Ar I line also decreased in Fig. 2, but the argon ion emission (Ar II), surprisingly, exhibited very small changes even as the amount of argon was changed substantially.

The emission intensities of the 380.5 –nm (0,2) bandhead of the second positive system (SPS) of N_2 ($C^3\Pi \rightarrow B^3\Pi$) decreased with increasing x(H_2), as shown in Fig. 2. The 375.5 –nm (1–3) bandhead intensity (not shown) had exactly the same behaviour as the 380.5 nm emission. As the actinometer concentration was constant during the experiments, the changes in emission intensities of the SPS of N_2 illustrate an influence of the increased H_2 partial pressure on the excitation efficiency of the electronically excited state $C^3\Pi$ of N_2, which is discussed below.

Main Excitation Channels

The range of possible elemental processes and chemical reactions that can occur in the discharge of the ternary Ar-H_2-N_2 mixtures is very large. The OES data cannot clearly distinguish among all possible ways to produce the optical emission. In the following interpretation of the OES results and in the consideration of the applicability of nitrogen as an actinometer for H-atom density, only reactions that appear dominant on the basis of the literature data are considered. Recombination and quenching processes are not discussed.

Regarding atomic hydrogen emission, the major mechanisms of production and excitation of H atoms believed to be present in low-pressure glow discharge devices are:

Table 1 Spectroscopic data of optical transitions measured [16, 17]

Species	Wavelength (nm)	Transitions	Threshold energy (eV)
H	486.1	4d–2p	12.74
	656.3	3d–2p	12.09
Ar (Ar I)	675.3	$4d_3$–$2p_{10}$	14.74
	687.1	$4d_5$–$2p_{10}$	14.71
	693.8	$4d_5$–$2p_{10}$	14,69
	696.5	$2p_2$–$1s_5$	13.32
	706.7	$2p_3$–$1s_5$	13.29
	710.7	$3p_5$–$2p_8$	14.84
	714.7	$2p_4$–$1s_5$	13.28
	720.7	$3s_2$–$2p_3$	15.01
	727.3	$2p_2$–$1s_4$	13.33
	731.2	$3s_4$–$2p_7$	14.85
	731.6	$3s_2$–$2p_2$	15.02
	735.3	$4d_4$–$2p_8$	14.84
	738.4	$2p_3$–$1s_4$	13.30
	750.4	$2p_1$–$1s_2$	13.47
	751.5	$2p_5$–$1s_4$	13.27
	811.5	$2p_9$–$1s_5$	13.07
Ar^+(Ar II)	459.0	4p–4s	21.12
Si (Si I)	288.2	$3p4s$–$3p^2$	5.08
Si^+ (Si II)	634.7	4p–4s	10.07
N_2	375.5	$C^3\Pi \rightarrow B^3\Pi$ (1 − 3)	11.5
	380.5	$C^3\Pi \rightarrow B^3\Pi$ (0 − 2)	11.2
CH	431.4	$A^2\Delta \rightarrow X^2\Pi$ (0 − 0)	2.9; ∼ 11[a]

[a] The threshold energy for CH considering various excitation processes

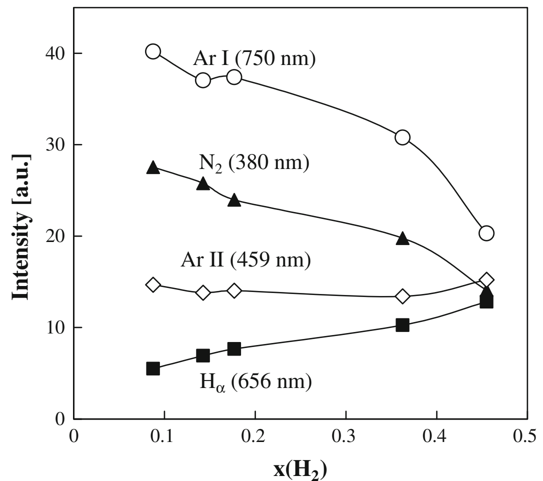

Fig. 2 Dependence of emission intensities of selected *spectral lines* and bands on H_2 amounts in an Ar-H_2 plasma. Discharge current 100 mA. The *solid lines* result from software smoothing

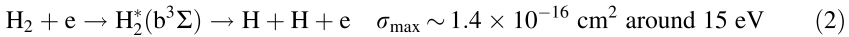

$$H_2 + e \rightarrow H_2^*(b^3\Sigma) \rightarrow H + H + e \quad \sigma_{max} \sim 1.4 \times 10^{-16}\ cm^2 \text{ around } 15\ eV \tag{2}$$

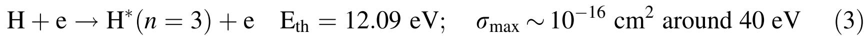

$$H + e \rightarrow H^*(n = 3) + e \quad E_{th} = 12.09\ eV; \quad \sigma_{max} \sim 10^{-16}\ cm^2 \text{ around } 40\ eV \tag{3}$$

$$H_2 + e \rightarrow H^*(n = 3) + H + e \quad E_{th} = 19\ eV; \quad \sigma_{max} \sim 10^{-18}\ cm^2 \text{ around } 70\ eV \tag{4}$$

where the star (*) symbol denotes electronic excitation states that result in optical emission. The cross section (σ_{max}) data and the threshold energies E_{th} are cited from Ref. [18].

In an argon–hydrogen glow discharge, other possible channels for formation of excited hydrogen atoms H^* are connected with the argon metastable species, Ar_m, and the Ar^+ ions according to the following reactions:

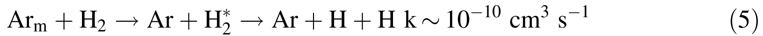

$$Ar_m + H_2 \rightarrow Ar + H_2^* \rightarrow Ar + H + H \ k \sim 10^{-10}\ cm^3\ s^{-1} \tag{5}$$

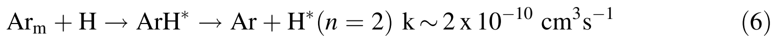

$$Ar_m + H \rightarrow ArH^* \rightarrow Ar + H^*(n = 2) \ k \sim 2 \text{ x } 10^{-10}\ cm^3 s^{-1} \tag{6}$$

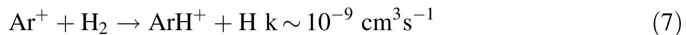

$$Ar^+ + H_2 \rightarrow ArH^+ + H \ k \sim 10^{-9}\ cm^3 s^{-1} \tag{7}$$

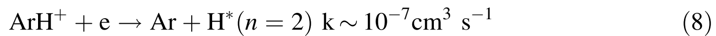

$$ArH^+ + e \rightarrow Ar + H^*(n = 2) \ k \sim 10^{-7} cm^3\ s^{-1} \tag{8}$$

The reaction rate coefficients (k) are from Ref. [18].

Based on the literature, the direct influence of the argon species on the dissociation of H_2 via reaction (5) and (7) is expected; however, the excitation of hydrogen atoms is probably mainly due to the direct electron impact excitation process (reaction (3)) and the electron impact dissociative excitation (reaction (4)) in decreasing order of importance [14, 19, 20]. From Ref. [14], the dissociative excitation process becomes competitive with the direct electron impact at a high electron temperature (see also E_{th} and σ_{max} for reaction (4)).

The emission from argon atoms is determined predominantly by direct electron impact excitation from the ground state:

$$Ar + e = Ar^* + e, \tag{9}$$

and/or by excitation of the atoms in metastable levels:

$$Ar_m + e = Ar^* + e. \tag{10}$$

The metastable atoms can be also ionised by electron collisions, which can be a source of argon ions in the plasma:

$$Ar_m + e = Ar^+ + e + e. \tag{11}$$

The emitting states of Ar^+ are produced by a two-step process, the first of which is ionization. Alternatively, these excited states can be produced from the single-step electron impact ionization and excitation of ground state Ar.

For the discharge conditions under study, when one considers the production of the $N_2(C^3\Pi)$ radiative state, the following most efficient reactions should be taken into account:

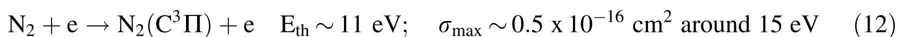

$$N_2 + e \rightarrow N_2(C^3\Pi) + e \quad E_{th} \sim 11\ eV; \quad \sigma_{max} \sim 0.5 \text{ x } 10^{-16}\ cm^2 \text{ around } 15\ eV \tag{12}$$

where the σ_{max} and E_{th} are cited from Ref. [21], and

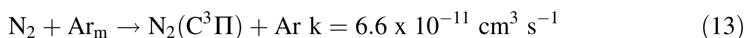

$$N_2 + Ar_m \rightarrow N_2(C^3\Pi) + Ar \ k = 6.6 \text{ x } 10^{-11}\ cm^3\ s^{-1} \tag{13}$$

where the rate coefficient k is cited from [22].

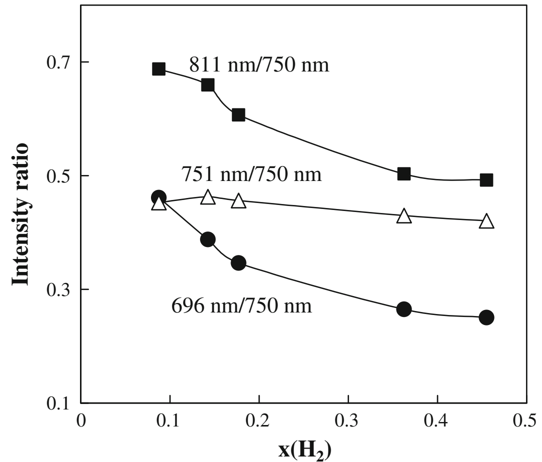

Fig. 3 Intensity ratios of the Ar I lines at 696.5, 751.5 and 811.5 nm to the Ar I–750.4 nm intensity

The relative contribution of processes (12) and (13) to the population of the $N_2(C^3\Pi)$ state is crucial for the validity of the N_2 actinometry procedure. For actinometry to be valid, certain electronically excited states of the actinometer and the species to be interested should be dominantly produced through direct electron-impact excitation of the corresponding ground state atoms (or molecules). In order to gain some insight into the importance of the processes involving the argon metastable atoms, we have analysed the emissions arising from the excited levels, which differ in efficiency of excitation out of the metastable levels of argon ($Ar_m + e \rightarrow Ar^* + e$). The Ar I lines at 750.4 and 751.5 nm have relatively small electron cross-section for excitation from the metastables ($\sigma_{max} < 0.73 \times 10^{-16}$ cm^2 and $\sigma_{max} \sim 0.44 \times 10^{-16}$ cm^2, respectively [23]). The Ar I 696.5 nm and Ar I 811.5 nm emissions arise from the levels most efficiently populated out of the metastable levels ($\sigma_{max} \sim 8.6 \times 10^{-16}$ cm^2 and $\sigma_{max} \sim 25 \times 10^{-16}$ cm^2, respectively [23]). Figure 3 shows intensity ratios of the Ar I lines at 696, 751 and 811 nm to the intensity of the 750 nm line, as a function of $x(H_2)$. It can be seen that the ratio I_{751}/I_{750} does not essentially change, whereas the I_{811}/I_{750} and I_{696}/I_{750} ratios fall with increasing $x(H_2)$. This indicates that stepwise excitation through metastable levels causes differences in the behaviour of the argon lines. The results in Fig. 3 suggest that an increase in $x(H_2)$ corresponds with a decrease in the relative contribution of the metastable states of argon in the plasma processes. This contribution is reduced, apparently, due to the depletion of argon metastables *via* reaction (5) and (6), as has been reported in Refs. [18–20].

Referring back to N_2 emissions, population of the $N_2(C^3\Pi)$ state *via* the reaction (13) cannot be excluded, but that contribution should considerably decrease with increasing hydrogen concentration.

Evolutions of the Plasma Parameters and Emission of the Actinometer

In an effort to derive information about the electron number density (N_e) in the plasma system studied, we used the full-width at half-maximum (FWHM) of the H_β line and the Griem formula [24]. The FWHM was calculated from a Lorentzian fit of the line peak. The absolute electron density values gained here can have large errors, but at this point, we are only interested in the qualitative effects. The standard deviation of the N_e determination was about 5%. It was found that as the $x(H_2)$ increased, the N_e decreased. This result is

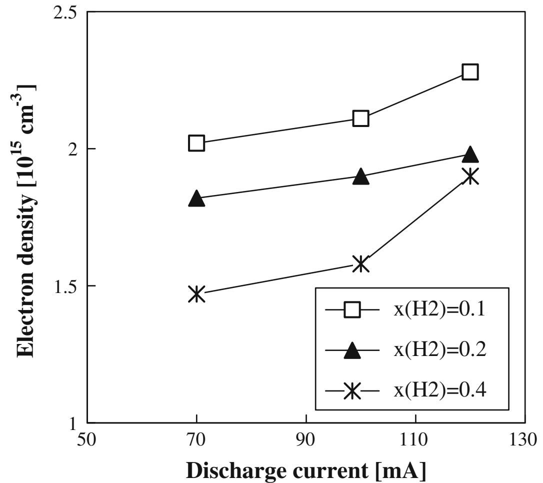

Fig. 4 Electron number density as determined from the FWHM of the H_β line as a function of the discharge current at different Ar/H_2 mixture compositions

consistent with the numerical investigations of an argon–hydrogen discharges [18, 20]. The effect of discharge current was also investigated. The increasing discharge current, over the range 70–120 mA, increased the electron density almost linearly. A summary of the N_e values is presented in Fig. 4 for plasmas of differing argon/hydrogen ratios.

Figure 5 shows how the electron number density alters the emission of the actinometer, depending on the hydrogen amount in an Ar-H_2 discharge. The intensity of the (0,2) vibrational band of N_2 ($\lambda = 380$ nm) is plotted versus N_e. The data points are for the three values of x(H_2) and the discharge currents (70, 100 and 120 mA). As can be seen, we found two distinct linear correlations: one for the plasmas at x(H_2) = 0.1 and x(H_2) = 0.2, and the other for hydrogen-rich plasma at x(H_2) = 0.4. These results are consistent with conditions in which electron impact excitation plays a predominant role as an excitation mechanism for the molecular nitrogen (reaction (12)). The existence of the two distinct slopes in Fig. 5 may be the result of considerable differences between the hydrogen-rich plasma and the plasmas at x(H_2) = 0.1 and x(H_2) = 0.2 in the electron temperature (the energy of electrons) responsible for the excitation process.

To obtain information concerning the tendencies of variations of the electron temperature, T_e, under the conditions studied here and to understand the results in Fig. 5, we have determined the excitation temperature (T_{exc}) of atomic argon from a Boltzmann plot of the $\ln(I\lambda/g_kA_{ki})$ versus the energy of level E_k, where I, λ, g_k, and A_{ki} are the intensity, wavelength, statistical weight, and transition probabilities from the k-level, respectively [24]. The 13 Ar I lines (675.3; 687.1; 693.8; 696.5; 706.7; 710.8; 714.7; 720.7; 727.3; 731.2; 731.6; 735.3; 738.4 nm) were measured to plot the Boltzmann diagram. The necessary parameters of g_k and A_{ki} for the lines were taken from the NIST database [17]. Figure 6 shows examples of the Boltzmann plot corresponding to the experiments carried out. The results of the T_{exc} calculation for the conditions in Fig. 5 are given in Table 2. From the data in Table 2, the discharge current, which influenced N_e, did not change or only slightly changed T_{exc}. However, as can be seen, the values of T_{exc} for x(H_2) = 0.4 are higher than the nearly equal one obtained at x(H_2) = 0.1 and 0.2. Owing to the high excitation thresholds of the Ar I lines considered here (13–15 eV, see Table 1), changes in the excitation temperature evaluated in this experiment can be linked to changes in the electron temperature of the hot electrons (electrons at the tail of the non-Maxwellian

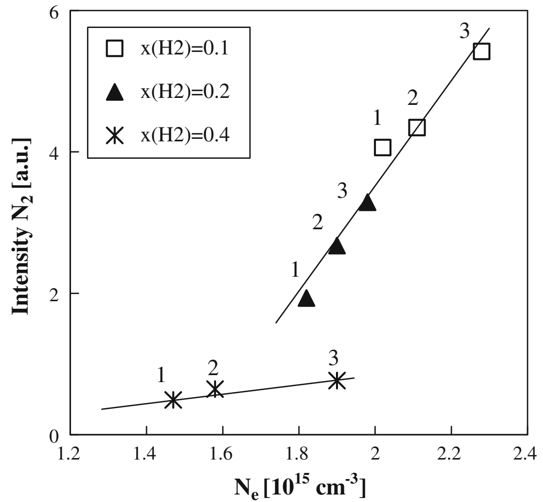

Fig. 5 Correlation between the emission intensity of the N_2 transition at 380 nm and the electron number density for plasmas of differing hydrogen amounts. Data points (1), (2) and (3) correspond to discharge currents 70, 100 and 120 mA, respectively

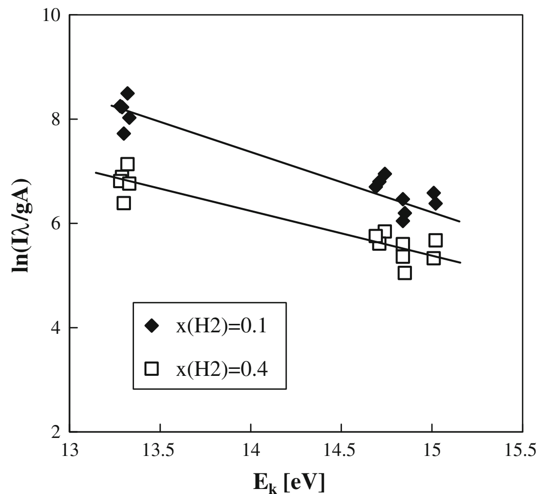

Fig. 6 Boltzmann plots for Ar I lines. Discharge current 100 mA

Table 2 The excitation temperatures with their uncertainties (in K) derived from argon lines

Current (mA)	$x(H_2) = 0.4$	$x(H_2) = 0.2$	$x(H_2) = 0.1$
70	14700 ± 1800	11400 ± 1400	11400 ± 1400
100	14000 ± 1600	11800 ± 1500	11600 ± 1500
120	14000 ± 1400	11900 ± 1600	12000 ± 1500

electron energy distribution function). Such an approach has been used for studying microwave plasma used for growing diamonds (pressure above 15 Torr) [14]. If this approach is accepted, the obtained T_{exc} suggests an expansion of the electron energy distribution function (EEDF) towards higher energies as the H_2 portion in the plasma increases up to 40%. Consequently, the electron-impact excitation efficiency towards N_2^*

(E_{th} ~ 11 eV) is reduced, which may explain the low intensity of the N_2 ($C^3\Pi \rightarrow B^3\Pi$) emission at $x(H_2) = 0.4$, as shown in Fig. 5.

Actinometric Determination of the Atomic Hydrogen Concentration

Considering the above analysis, there is strong evidence that the emission of N_2 measured here is highly sensitive to changes in electron density (N_e) and temperature (T_e), and it can play the role of an actinometer, sensing changes in electron-impact excitation efficiency for excitation thresholds at about 11 eV. The emitting states of N_2 ($C^3\Pi$, $v' = 0$) and H ($n = 3$) are close in threshold energy (11.2 and 12.09 eV, respectively), thereby satisfying the requirement for actinometric determination of the H-atom. However, in the plasma under study, the ideal actinometry conditions are rather questionable. The validity of actinometry may be critical for the following conditions:

- at a high concentration of argon, the possibility of $N_2(C^3\Pi)$ population via transfer of internal energy from Ar_m atoms to the ground state of the nitrogen molecule (reaction (13)) cannot be excluded;
- at a high concentration of hydrogen, the electron temperature is probably high, and the possibility of a contribution of the dissociative excitation of H_2 to the production of excited H atoms could produce misleading actinometry results (reaction(4));
- a high contribution of quenching of the excited states by nonradiative processes due to relatively high pressure under these experimental conditions.

Considering the above limitations, variations (with changing experimental conditions) in the relative H-atom concentration, [H], as determined from the actinometric dependence [H] ~ I_H/I_{N2}, will be considered.

Figure 7 shows the relative H-atom concentration as a function of $x(H_2)$, at the discharge current 100 mA. The results are derived from the ratios of the Balmer H_α ($E_{th} = 12.09$ eV) and H_β ($E_{th} = 12.74$ eV) lines to the N_2 transition at 380.5 nm ($E_{th} = 11.2$ eV). It is seen that the ratios both increase with hydrogen amount in the feed in an identical fashion. An increase of H-atom mole fraction by more than two times as the H_2

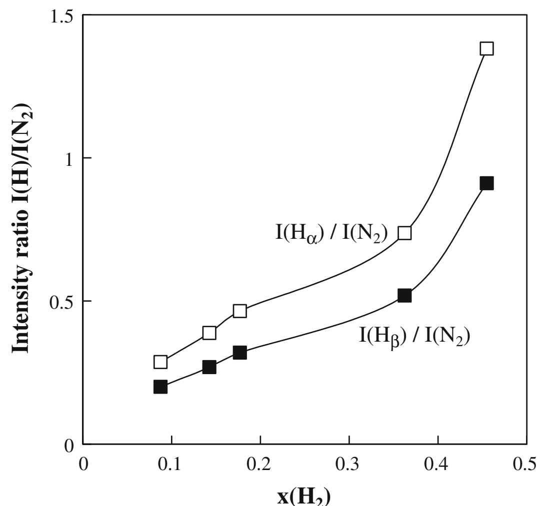

Fig. 7 Evolution of the relative density of hydrogen atoms versus H_2 amount in an Ar-H_2 plasma determined from the ratio of H_α and H_β to N_2–380 nm intensities. Discharge current 100 mA. The *solid lines* result from software smoothing

portion increases by four times, from $x(H_2) = 0.09$ to 0.36, has been found. Between $x(H_2) = 0.36$ and 0.45, the increase is more pronounced, but keeping in mind the limitations of validity of actinometry, we consider that the results for $x(H_2) = 0.45$ are probably overestimated.

In summary, the principal results of this OES investigation on 100-kHz discharge in an argon–hydrogen mixture at a total pressure of 665 Pa (5 Torr) indicate that:

- an increasing fraction of hydrogen in the feed results in a decrease in the electron number density;
- as the H_2 portion in the plasma increases up to 40%, the number of high-energy electrons is enhanced;
- it is quite plausible to use nitrogen, i.e., the N_2 ($C^3\Pi \rightarrow B^3\Pi$) emission, as an actinometer for determining H-atom concentration variations in the plasma;
- the relative H-atom density determined by actinometry continuously increases with $x(H_2)$ for $x(H_2) = 0.9$–0.45.

CH_3SiCl_3–Ar–H_2 Plasma System

The emission spectra of the discharge in methyltrichlorosilane-argon–hydrogen mixtures consisted of Ar I, Ar II and H lines, as observed before in an argon–hydrogen plasma, and additionally: Si I lines (251.4; 251.6; 252.4; 252.8; 288.2 nm), Si II lines (634.7 and 637.2 nm) and the CH ($A^2\Delta$–$X^2\Pi$) band at 431.4 nm. An interesting feature to be noticed in the spectra was significant broadening of the Si II lines. Typical emission spectrum of the CH_3SiCl_3–Ar–H_2 plasma in the 410–435 nm wavelength range is shown in Fig. 8.

In preliminary experiments, conducted at higher MTCS flows than applied here, the emission from the SiCl molecule (the main systems $B^2\Sigma$–$X^2\Pi$ and $B^2\Delta$–$X^2\Pi$) was detected. The appearance of the C I line (at 247.8 nm) and SiH band (at 414.2 nm) was expected, but these spectra have not been found.

Intensities of the following emissions, Si I (288.2 nm), Si II (634.7 nm), CH (431.4 nm), H (486.1 nm, 656.3 nm), Ar I (751.5 nm), Ar II (459.0 nm) and additionally the emission of N_2 (380.5 nm) and N_2^+ (427.8 nm) coming from the nitrogen that was introduced as an actinometer, were measured as a function of time following introduction of the MTCS to an argon–hydrogen plasma. The spectroscopic data of the measured optical transitions are

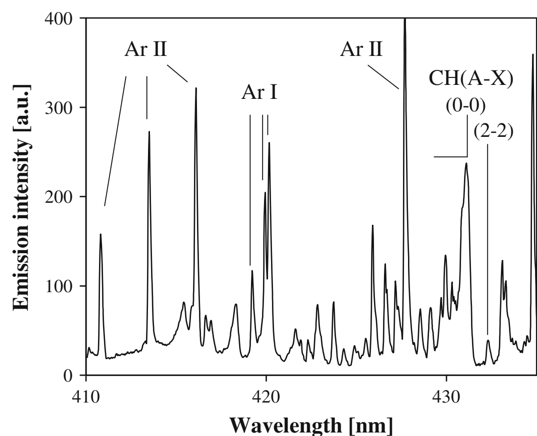

Fig. 8 Typical emission spectrum in the 410–435 nm region from the discharge in the MTCS-Ar-H_2 mixture

shown in Table 1. The spectra were recorded over about 1 h of the experiment conducted continuously, with a constant value of discharge current of I = 100 mA, for three Ar + H_2 mixture compositions correspond to x(H_2) = 0.1, 0.2 and 0.4.

An acquisition of the OES data was stated 8 min after the MTCS was introduced, in order to avoid the initial plasma disturbance mentioned above, and it was repeated six times at intervals step of 10 min. Because a single acquisition run took about 2 min, various wavelengths were measured at different times (but the same wavelengths were measured at the same time) from the beginning of the experiment. It is reasonable to suppose that major changes of the discharge composition due to the introduction of the MTCS occurred within the initial interval ($t < 8$ min), which unfortunately could not be examined due to the lack of stability of the discharge process. So far, this experimental problem remains unsolved. The systematic uncertainties in the measurements were estimated to be less than 5%. To improve the legibility of the following figures, the error lines are not presented.

Emission from the Plasma Gas Species

As a first point, the intensity of the actinometer emission at 380.5 nm is reported in Fig. 9 as a function of time of the experiments at x(H_2) = 0.1, 0.2 and 0.4. Independent of the feed gas composition, a decrease in the N_2 intensity can be observed in about the first 20 min, followed by a relatively slow decay or by saturation in the intensity.

Figure 9 depicts the dependence on x(H_2) as observed earlier for the Ar-H_2 plasma: a decrease in intensity with the hydrogen dilution. However, compared with the results in Fig. 2 for the Ar-H_2 plasma, in the case of the MTCS-Ar-H_2 plasma there is a greater difference in relative intensities of the N_2 emission at x(H_2) = 0.1 and x(H_2) = 0.2.

If it is assumed that the actinometry technique remains valid in the mixtures with MTCS addition, then Fig. 9 gives an idea of the extent of changes in the plasma activity due to the addition of MTCS and to the time of the experiment. The changes in the monitoring OES signal of N_2 should be related to changes in electron density and/or electron temperature. In order to investigate this question further, the T_{exc} and N_e were estimated, as previously

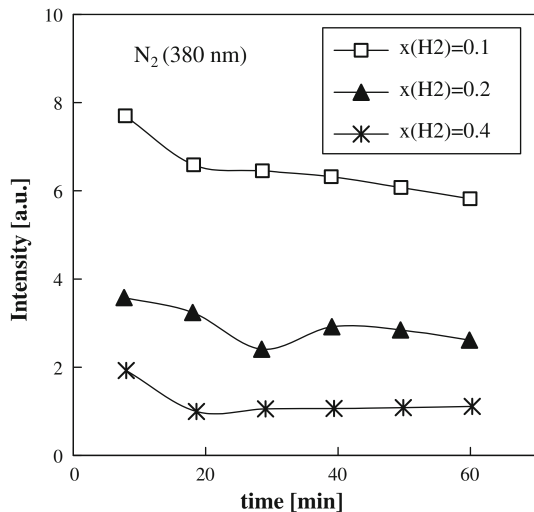

Fig. 9 Optical emission intensity of N_2 as a function of the time of the experiments

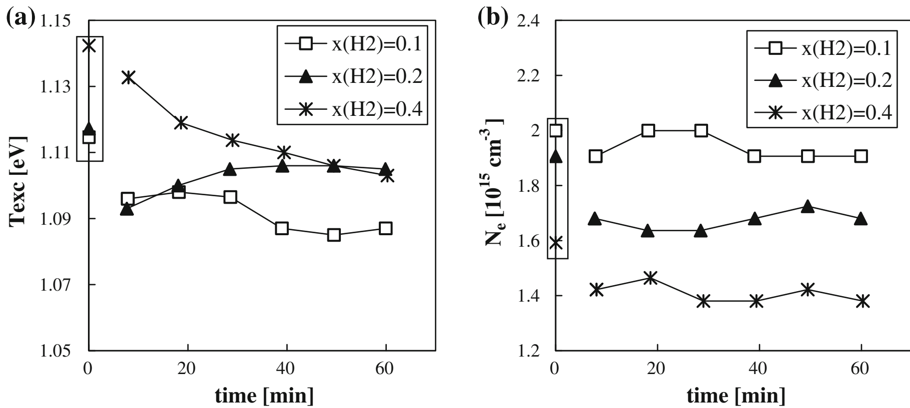

Fig. 10 Excitation temperature (**a**) and electron number density (**b**) in the MTCS-Ar-H_2 plasmas as a function of the time of the experiments. The data at $t = 0$ are for an Ar-H_2 plasma

for an Ar-H_2 plasma. The results are collected in Fig. 10a and b. In these figures, the data at $t = 0$ are for an argon–hydrogen (+N_2) plasma (without MTCS). It can be seen that the T_{exc} and the electron density both decreased as the MTCS was injected into an argon–hydrogen discharge. The T_{exc} values seemed to vary further with time, while the N_e kept almost a constant value (taking into account the error of about 5%).

The results for T_{exc} indicate that the decomposition process of the MTCS molecule involved a cooling effect of the electron temperature, which is generally consistent with the findings of others authors [25, 26]. It should be remembered that in plasmas with low electron temperature, the number of electrons above the excitation threshold, that is usually about 10 eV or higher, increases exponentially with the T_e. Therefore, small changes of T_e can cause important changes in the densities of excited species.

Considering the reason for a decrease of the electron density due to the MTCS addition, the following reaction should be taken into account:

$$SiCl_x + e \rightarrow SiCl_{x-1} + Cl^-, \quad \text{where } x = 1 - 3. \tag{14}$$

As discussed by Mogensen et al. [27] for the PACVD of TiN from the dc $TiCl_4$/Ar/H_2/N_2 plasma, the large electron affinity (3.61 eV) of Cl, makes it very probable that Cl immobilises free electrons by dissociative attachment and, consequently, that reactions like (14) have a considerable effect on the density of electrons. The $SiCl_3$ radical in reaction (14) is obviously the product of dissociation of MTCS in the plasma (Si–C bond is the weakest in the MTCS molecule [28]). The dissociation is most probably caused by:

– collisions of MTCS with electrons

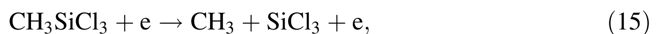

$$CH_3SiCl_3 + e \rightarrow CH_3 + SiCl_3 + e, \tag{15}$$

– eventually by collisions with argon metastables [29]

$$CH_3SiCl_3 + Ar_m \rightarrow CH_3 + SiCl_3 + Ar \tag{16}$$

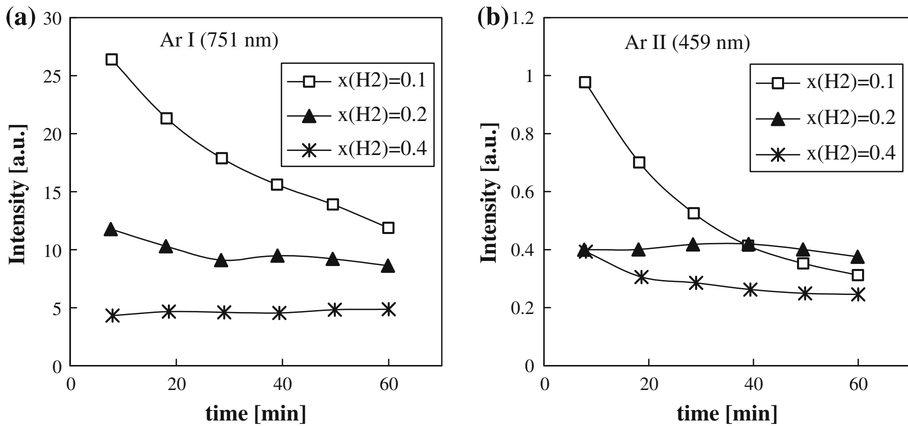

Fig. 11 Emission intensities of Ar I (**a**) and Ar II (**b**) *spectral lines* as a function of the time of the experiments with the MTCS-Ar-H_2 mixtures

Figure 11a and b show variations in the emission intensities of the Ar I and Ar II spectral lines, respectively, versus time of the experiments at $x(H_2) = 0.1$, 0.2 and 0.4. As can be seen, at the largest quantity of Ar in the gas feed ($x(H_2) = 0.1$), these lines show exponential-like decreases in intensity with time. At $x(H_2) = 0.2$ as well as $x(H_2) = 0.4$, the evolution of intensities of the Ar I and Ar II are comparatively very small.

The time dependence of the H_α emission for the three mixtures studied is reported in Fig. 12a. One can see that at $x(H_2) = 0.4$, the H_α intensity decreased with time, while at $x(H_2) = 0.2$ an initial enhancement in the intensity followed by a slow decay was found. As a result, during experiments with MTCS, the more intense emission of the H_α was observed at $x(H_2) = 0.2$ compared to that at $x(H_2) = 0.4$. The same behaviour was observed for the H_β line. The relevant dependencies of the H_α line intensity normalized to the intensity of the N_2 emission, i.e. actinometric densities of atomic hydrogen, are shown

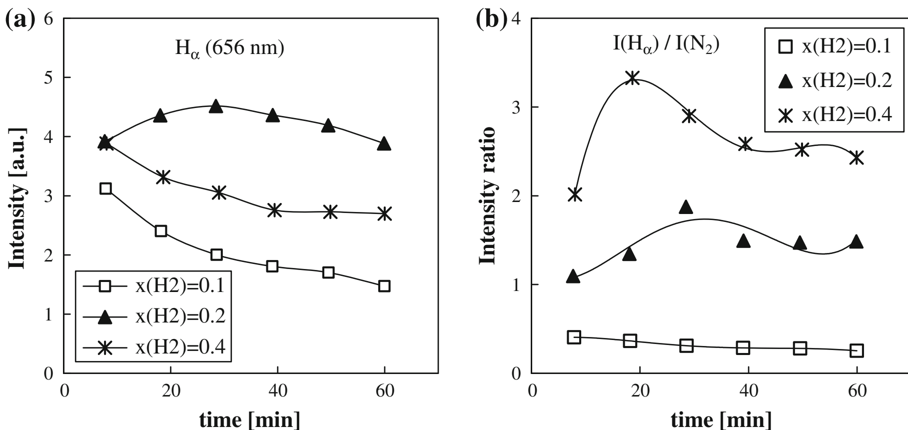

Fig. 12 H_α emission intensity (**a**) and H_α emission intensity normalized to the emission from N_2 at 380 nm (**b**) versus time of the experiments

in Fig. 12b. As expected, the value of the $I(H_\alpha)/I(N_2)$ ratio increased with the amount of H_2 in the feed. At $x(H_2) = 0.1$, the ratio decreased slowly with time. For the mixtures containing 20 and 40% of H_2, an increase of the $I(H_\alpha)/I(N_2)$ ratio up to a maximum value after 20–30 min from the beginning of the experiments was observed. These latter results were intriguing.

Unlike in an argon–hydrogen plasma, the data on Fig. 12b may be unreliable regarding the relative concentration of H atoms present in the plasma, since the dissociative excitation of hydrogen atoms out of the MTCS or its fragments could cause misleading actinometry results. Our experiments do not obtain information on this question, but we refer to the results obtained by Welzel and co-workers [30]. They have found that if H_2 is introduced together with $Si(CH_3)_4$, Ar and N_2 to the ECR plasma source, the dissociation of H_2 is dominant for the production of hydrogen atoms. For this reason, we reject the possibility of excited H production from CH_3SiCl_3 dissociation and assume that the results in Fig. 12b represent the H-atomic density variations, showing a real excess atomic hydrogen generation during our experiments with MTCS/Ar/H_2 mixture when hydrogen amount $x(H_2)$ was 0.2 and 0.4.

The results in Fig. 12b are reminiscent of previous actinometric studies of atomic hydrogen concentration in diamond PACVD using H_2/Ar/CCl_2F_2 or H_2/Ar/CCl_4 mixtures [31, 32]. Their authors reported enhanced atomic hydrogen production with halocarbons in the plasma. For 5% CCl_2F_2 in the feed, an increase of around 200% in the atomic hydrogen concentration was obtained and it has been suggested that the dissociation process of the halocarbons associated with HCl and/or HF formation followed by the dissociative-attachment process $e + HCl \rightarrow H + Cl^-$ and $e + HF \rightarrow H + F^-$ is responsible for the increase of the atomic hydrogen concentration. It is possible that the HCl dissociation also contributes to our results. Exhaust gas analysis confirmed the presence of HCl in our plasma reactor. Therefore, if this was the case in our experiment, an increase in hydrogen atom concentration can be related to a sequence of events such as:

1. dissociation of CH_3SiCl_3 into CH_3 and $SiCl_3$ (reaction (15) and (16))
2. reaction between H_2 and $SiCl_x$ ($x = 1$–3) radical with the production of $SiCl_{x-1}$, HCl and additional H atom

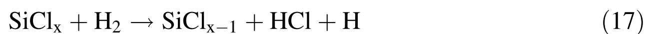

$$SiCl_x + H_2 \rightarrow SiCl_{x-1} + HCl + H \quad (17)$$

3. electron-impact dissociation of HCl molecule, e.g.,

$$e + HCl \rightarrow H + Cl^- \quad (18)$$

In this mechanism, the H-atom density depends strongly on the H_2 concentration in the feed. Six atoms of H may be formed per MTCS molecule (and three H_2 molecules). We think that the above mechanism explains the experimental results of Fig. 12b.

Si, Si^+ and CH Emission Analysis

Figure 13 illustrates the evolution of the emission intensity of the Si I spectrum with experimental time for the three mixtures studied. The emission from silicon atoms was observed to decrease rapidly with time. It is interesting that the emission was the most intensive when $x(H_2)$ was 0.2, suggesting that there may be an optimum value of the H_2 concentration in the feed gas with a subsequent high plasma activity to produce excited silicon atoms in the plasma.

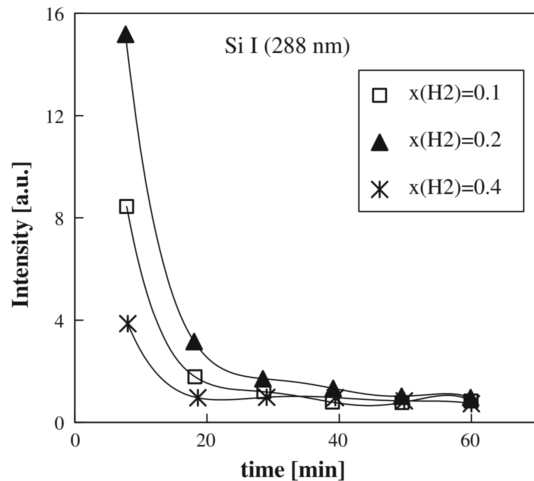

Fig. 13 Evolution of the relative intensity of the Si I emission *versus* time of the experiments

The results in Fig. 13 can be accounted for by assuming that the Si emission is affected predominantly by the partial pressure of the MTCS, but controlled mainly by electron density and temperature, with hydrogen playing an important role in the fragmentation of the $SiCl_x$ radicals, according to reaction (17). The higher N_e and energy not only allows an enhanced dissociation of the MTCS in general (reaction (15)), but additionally promotes the dissociation down to a small fragmentation pattern and the silicon atom (reaction (14)). Silicon atoms originated in this way can be excited by collisions with electrons ($E_{th} \sim 5$ eV).

There is no good actinometer for the low-energy electron-impact excitation of such species as silicon atom. However, we can reasonably assume that the concentration of silicon atoms in their ground state decreased with time in a similar way to the observed emission intensities of the Si I. Therefore, at the initial stage of the experiments, a high amount of atomic silicon in the plasma would be expected, but after about 20 min of continuous experiments, the density of Si in the plasma discharge is reduced to a low concentration. This decrease is likely due to increased depletion of Si atoms through homogeneous recombination and wall recombination. With increasing time of experiment, one would expect that the concentration of radicals adsorbed on the walls available for recombination would increase, giving a rise in recombination rates.

The emission intensity of ionic silicon (not shown) did not track the emission of atomic silicon, but followed the behaviour of the CH emission shown in Fig. 14. As can be seen, the CH emission decreased with time, but not so suddenly as the Si I emission, particularly in the case of the mixture consisting of 20 and 40% H_2.

In Fig. 15, the intensity of CH is plotted against that of Si II. The data shown are for different $x(H_2)$ concentrations and different times of the experiments. As can be seen, there is a clear correlation between CH (431.4 nm) and Si II (634.7 nm) emission over the wide range of process conditions covered in these measurements. The relationship can be represented by one line dependence regardless of different $x(H_2)$ values as well as of the time of the measurement.

The results in Fig. 15 suggest close similarity in the pathways responsible for the CH and Si^+ emissions. Considering the CH emission, the major production process of the

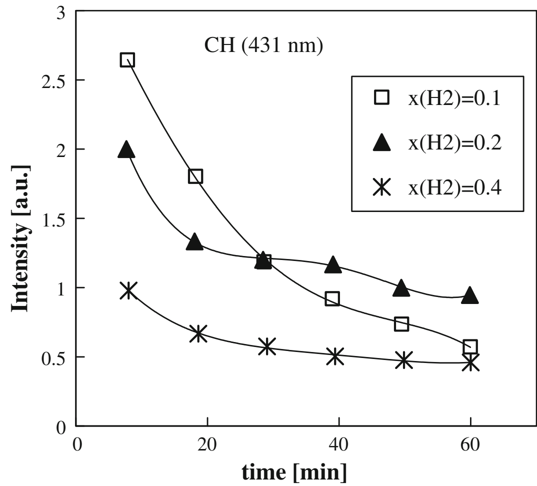

Fig. 14 Evolution of the relative intensity of the CH emission versus time of the experiments

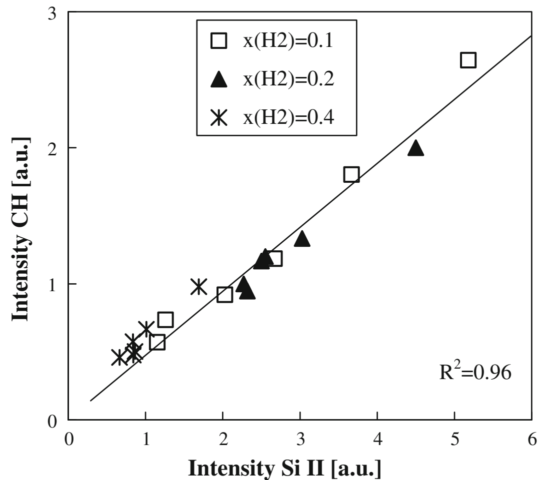

Fig. 15 Correlations between optical emission intensities of the CH at 431 nm and the Si II at 634.7 nm

excited $CH(A^2\Delta)$ radicals is assumed to be dissociative excitation by electron collision processes with CH_3 as follows:

$$CH_3 + e \rightarrow CH(A^2\Delta) + H_2 + e \; E_{th} \sim 11 \text{ eV} \quad (19)$$

The CH radical can also be directly excited by low energy electrons

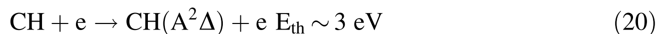

$$CH + e \rightarrow CH(A^2\Delta) + e \; E_{th} \sim 3 \text{ eV} \quad (20)$$

However, process (20) is usually neglected as a source of the $CH(A^2\Delta)$ due to the large destruction rate of CH radicals by radical-molecule reactions, which makes their number density in the plasma much smaller than that of CH_3 [33]. Accordingly, the emission intensity of CH $A^2\Delta \rightarrow X^2\Pi$ can provide information on the production process of the CH_3 radical, since the intensity is proportional to $k_{CH}N_e[CH_3]$, where k_{CH} is the excitation rate constant and $[CH_3]$ is the CH_3 density. The methyl radicals result from fragmentation of the MTCS molecule by electron impact and eventually from interactions with Ar atoms

in metastable states, as mentioned earlier. On the other hand, the CH_3 radicals can be lost by electron impact dissociation, diffusion towards the wall, or radical-molecule reactions. The contribution of the loss processes to the density of the CH_3 is considered to be almost constant with changes in the composition of the feed gas because the pressure and the MTCS flow were fixed.

Generally, the above mechanism involving the processes of electron impact fragmentation and excitation, is in agreement with the experimental results shown in Fig. 14, where the increase in the emission intensity of the CH $A^2\Delta \rightarrow X^2\Pi$ corresponds to increasing Ar fraction in the plasma feed gas, that is, the electron density (see Fig. 10b) and the Ar metastables.

The threshold energy for appearance of the CH($A^2\Delta$) in reaction (19) is not known. Usually it is approximated as 11 eV, which means that it is close to the threshold energy of the N_2 emission at 380.5 nm, $E_{th} = 11.2$ eV. Therefore, according to actinometry, the emission intensity ratio I(CH)/I(N_2) has been treated as proportional to the density of CH_3 species in the plasma. The rate of generation of the CH_3 radical can be expressed by $[CH_3] \propto k\, I_{CH}/I_{N2}$, where k is constant.

Figure 16 shows the intensity ratio of I(CH)/I(N_2) as a function of time of the experiments with the three MTCS/Ar/H_2 mixtures studied. Error bars, which are added to the data when $x(H_2) = 0.2$, reflect one standard deviation from the value due to error in optical emission intensity measurement. The uncertainty in each of the plotted points was less than 7%. At first sight, the results in Fig. 16 are unexpected because they are quite different from the dependencies found for the CH emission (Fig. 14). From the data in Fig. 16, it becomes apparent that the CH_3 density increased with higher hydrogen percentages in the feed. This result can be explained by increased H density in the plasma, which leads to an enhanced chemical sputtering of already deposited material and returns hydrocarbons to the discharge. Chemical sputtering is a highly effective erosion mechanism that must be considered when growing film that is simultaneously exposed to flux of energetic ions and of reactive neutrals. It was observed that the erosion rate of C:H films by low-energy Ar^+ ions is drastically enhanced if atomic hydrogen is also incident on the film surface, e.g. [34]. The mechanism of the chemical sputtering is assumed to be the formation of stable volatile products such as CH_4 that diffuse to the surface and desorb. The dissociation of

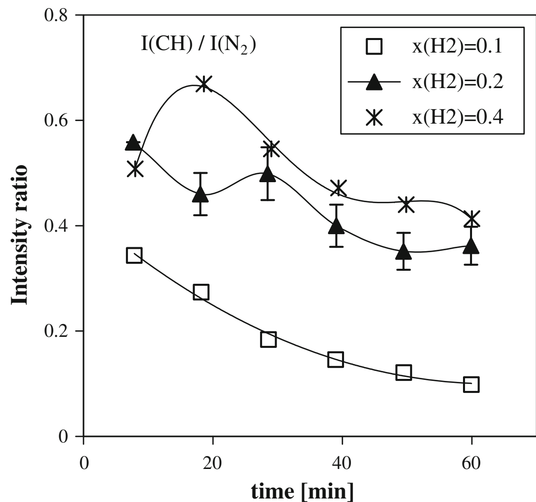

Fig. 16 CH emission intensity normalized to the emission from N_2 at 380 nm versus time of the experiments

these molecules can add to the CH_3 produced from MTCS, giving the results determined here by actinometry.

The fact that the Si II emission exhibited a very similar profile and behaviour to that of CH emission strongly suggested that the process of chemical sputtering significantly contributes to the production of Si^+ ions. It seems likely that the Si^+ emission observed here is associated with a secondary ionization, i.e., ionization of Si atoms or silicon containing species ejected from the cathode surface. The probability of ion ejection could be extremely low, as ions are inevitably attracted back to the surface. Therefore, the Si ions are created ($E_{ion} = 8.2$ eV) and excited ($E_{th} = 10$–12 eV) in the plasma. It is noteworthy that the threshold energies for the Si II and CH emissions observed here are very close, 10.1 eV and about 11 eV, respectively. In other words, the excited states of Si^+ and CH can be produced by electrons of similar energy, which can be important for the correlation between the emissions of these two excited species.

Concluding Remarks

An identification of the elementary reaction mechanisms in reactive plasmas used for PACVD processes is extremely difficult, if not impossible, as the number of possible gas phase reactions and processes on the growing film surface is too great. In this work, the production of active species in the CH_3SiCl_3-Ar-H_2 low frequency discharge has been analysed by optical emission spectroscopy and actinometry. The intensities of the optical spectra of Si I, Si II, CH, H, Ar I and Ar II are reported as a function of time following the introduction of CH_3SiCl_3 to the argon–hydrogen plasmas with various proportions of the feed gasses. The results show that plasmas with different concentrations of the excited species were generated at different times during the experimental measurements. These variations would influence the homogeneity of film growth in the discharge.

It is important to note that varying the H_2 content in the CH_3SiCl_3-Ar-H_2 source gas mixtures caused significant changes in the intensities of the Si, Si^+ and CH optical emissions. An analysis of the results indicates that the relative density of silicon atoms in the plasma is controlled mainly by the plasma activity (the electron number density and the shape of the EEDF), and that the Si^+ and CH densities are coupled to products of sputtering of the growing film surface. Valuable and practical information regarding the competition between the deposition and chemical sputtering of already deposited material may then be inferred from measurements of the Si II or CH spectra, and the results can be used to optimize the PACVD process.

At the present time, the available data do not allow us to have a more advance discussion on a deposition model of films made from the decomposition of methyltrichlorosilane/argon/hydrogen mixtures in a low frequency plasma device. We leave this matter for future discussion when more experimental data will be available.

Acknowledgments The authors wish to express their thanks to T Świda for his assistance in the experiments.

References

1. Grill A (1994) Cold plasma in materials fabrications. IEEE Press, New York
2. Foti G (2001) Appl Surf Sci 184:20–26

3. Hu Z, Liao X, Diao H, Kong G, Zeng X, Xu Y (2004) J Crys Growth 264:7–12
4. Ivashchenko LA, Rusakov GV, Ivashchenko VI (1999) Appl Surf Sci 138–139:444–448
5. Rusakov GV, Ivashchenko LA, Ivashchenko VI, Porada OK (2001) Appl Surf Sci 184:128–134
6. Porada OK, Rusakov GV, Ivashchenko LA, Ivashchenko VI, Popov VM, Dub SM (2005) Powder Metall Met Ceram 44:363–371
7. Porada OK, Ivashchenko VI, Ivashchenko LA, Rusakov GV, Dub SN, Stegnij AI (2004) Surf Coat Technol 180–181:122–126
8. Ivashchenko VI, Dub SN, Porada OK, Ivashchenko LA, Skrynskyy PL, Stegnij AI (2006) Surf Coat Technol 200:6533–6537
9. Kaneko T, Miyakawa N, Sone H, Yamazakia H (2001) Surf Coat Technol 142–144:360–364
10. Kaneko T, Nemoto D, Horiguchi A, Miyakawa N (2005) J Crys Growth 275:e1097–e1101
11. Coburn JW, Chen M (1980) J Appl Phys 51:3134–3136
12. d'Agostino R, Cramarossa F, De Benedictis S, Fracassi F (1984) Plasma Chem Plasma Process 4:163–168
13. Kogelschatz M, Cunge G, Sadeghi N (2006) Eur Phys J Appl Phys 33:205–212
14. Gicquel A, Chenevier M, Kh Hassouni, Tserepi A, Dubus M (1998) J Appl Phys 83:7504–7521
15. Jamróz P, Żyrnicki W (2005) Diam Relat Mater 14:1498–1507
16. Huber KP, Herzberg G (1979) Constants of diatomic molecules. Van Nostrand Reinhold Co, New York
17. NIST-Atomic Spectra Database, URL: http://www.physics.nist.gov/PhysRefData
18. Bogaerts A, Gijbels R (2000) J Anal At Spectrom 15:441–449
19. Stoltz AJ, Sperry MJ, Benson JD, Varesi JB, Martinka M, Almeida LA, Boyd PR, Dinan JH (2006) J Electron Mater 34:733–739
20. Bogaerts A (2002) J Anal At Spectrom 17:768–779
21. Itakawa Y, Hayashi M, Ichimura A, Onda K, Sakimoto K, Takayanagi K, Nakamura M, Nishimura H, Takayanagi T (1986) J Phys Chem Ref Data 15:985–1010
22. Bockel S, Amorim J, Baravian G, Ricard A, Stratil P (1996) Plasma Sources Sci Technol 5:567–572
23. Boffard JB, Piech GA, Gehrke MF, Anderson LW, Lin Ch C (1999) Phys Rev A 59:2749–2763
24. Griem HR (1964) Plasma spectroscopy. McGraw-Hill, New York
25. Cho BO, Lao S, Sha L, Chang JP (2001) J Vac Sci Technol A 19:2751–2761
26. Scordo S, Ducarroir M, Berjoan R, Jauberteau JL (1997) Chem Vap Deposition 3:119–128
27. Mogensen KS, Eskildsen SS, Mathiasen C, Bøttiger J (1998) Surf Coat Technol 102:41–49
28. Linde DR (Ed.) (1994) Handbook of Chemistry and Physics. 75th Ed CRC Press, Boca Raton
29. Jauberteau JL, Jauberteau I, Aubreton J (2000) Chem Phys Lett 327:351–358
30. Th Welzel, Dani I, Richter F (2002) Plasma Sources Sci Technol 11:351–359
31. Ferreira NG, Corat EJ, Trava-Airoldi VJ, Leite NF, Del Bosco E (1998) Diam Rel Mater 7:81–87
32. Ferreira NG, Corat EJ, Trava-Airoldi VJ, Leite NF (2000) Diam Rel Mater 9:368–372
33. Tachibana K, Nishida M, Harima H, Urano Y (1984) J Phys D Appl Phys 17:1727–1742
34. Hopf C, von Keudell A, Jacob W (2003) J Appl Phys 94:2373–2380